Mutual epithelium-macrophage dependency in liver carcinogenesis mediated by ST18

Micol Ravà[1], Aleco D'Andrea[2], Mirko Doni[2], Theresia R. Kress[1#], Renato Ostuni[2$], Valerio Bianchi[1†], Marco J. Morelli[1], Agnese Collino[2], Serena Ghisletti [2], Paola Nicoli[2], Camilla Recordati[3], Maria Iascone[4], Aurelio Sonzogni[5], Lorenzo D'Antiga[6], Ruchi Shukla[7‡], Geoffrey J. Faulkner[7,8], Gioacchino Natoli[2], Stefano Campaner[1] and Bruno Amati[1,2]*

[1] Center for Genomic Science of IIT@SEMM, Fondazione Istituto Italiano di Tecnologia (IIT), Via Adamello 16, 20139 Milan, Italy.

[2] Department of Experimental Oncology, European Institute of Oncology (IEO), Via Adamello 16, 20139 Milan, Italy.

[3] Mouse & Animal Pathology Laboratory, Fondazione Filarete, Viale Ortles 22/4, 20139 Milan, Italy.

[4] Medical and Laboratory Genetics, Azienda Ospedaliera Papa Giovanni XXIII, Piazza OMS 1, 24127 Bergamo, Italy.

[5] Pathology Department, Azienda Ospedaliera Papa Giovanni XXIII, Piazza OMS 1, 24127 Bergamo, Italy.

[6] Paediatric Liver, GI and Transplantation,☐Azienda Ospedaliera Papa Giovanni XXIII, Piazza OMS 1, 24127 Bergamo - Italy

[7] Division of Genetics and Genomics, The Roslin Institute and Royal (Dick) School of Veterinary Studies, University of Edinburgh, Easter Bush EH25 9RG, UK.

[8] Mater Research Institute - The University of Queensland, Translational Research Institute, Woolloongabba QLD 4102, Australia.

Current addresses:
[†] Hubrecht Institute-KNAW & University Medical Center Utrecht, Utrecht, The Netherlands.
[‡] Northern Institute for Cancer Research, Newcastle University, UK.
[$] San Raffaele Telethon Institute for Gene Therapy, Division of Regenerative Medicine, Stem Cells and Gene Therapy, IRCCS San Raffaele Scientific Institute, Milan, Italy.
[#] Department of Translational Medicine and Clinical Pharmacology, Boehringer Ingelheim Pharma GmbH&Co.KG, Biberach an der Riss, Germany.

* To whom correspondence should be addressed

Contact Information:

Dr. Bruno Amati

Center for Genomic Science of IIT@SEMM, Fondazione Istituto Italiano di Tecnologia (IIT) Via Adamello 16, 20139 Milan, Italy

Tel: +39 02 5748 9824

Fax: +39 02 9437 599

e-mail: bruno.amati@iit.it

Abbreviations:

ST18, Suppression of Tumorigenicity 18; HCC, hepatocellular carcinoma; NF-kB, Nuclear Factor kappa-B; *NZF-1, neural zinc finger factor-1; Myt1, myelin transcription factor-1; PFIC , progressive familial intrahepatic cholestasis; LPS, lipopolysaccharide; TAMs, Tumor-associated macrophages; IHC, Immunohistochemistry; GSEA, Gene Set Enrichment Analysis; L1, LINE-1; H&E, Hematoxylin and eosin.*

p. 2

Abstract

The *ST18* gene was proposed to act either as a tumor suppressor or as an oncogene in different human cancers, but direct evidence for its role in tumorigenesis was missing so far. Here, we demonstrate that *ST18* is critical for tumor progression and maintenance in a mouse model of liver cancer, based on oncogenic transformation and adoptive transfer of primary precursor cells (hepatoblasts). *ST18* mRNA and protein were detectable neither in the normal liver nor in cultured hepatoblasts, but were readily expressed following subcutaneous engraftment and tumor growth. *ST18* expression in liver cells was induced by inflammatory cues, including acute or chronic inflammation *in vivo*, as well as co-culture with macrophages *in vitro*. Knocking down the *ST18* mRNA in transplanted hepatoblasts delayed tumor progression. Induction of *ST18* knockdown in pre-established tumors, caused rapid tumor involution, associated with pervasive morphological changes, proliferative arrest and apoptosis in tumor cells, as well as depletion of tumor-associated macrophages, vascular ectasia and hemorrhage. Reciprocally, systemic depletion of macrophages in recipient animals had very similar phenotypic consequences, impairing either tumor development or maintenance, and suppressing *ST18* expression in the hepatoblasts. Finally, RNA-seq profiling of *ST18*-depleted tumors prior to involution revealed down-regulation of inflammatory response genes, pointing to the suppression of NF-kB-dependent transcription. *Conclusion:* ST18 expression in epithelial cells is induced by tumor-associated macrophages, contributing to the reciprocal feed-forward loop between both cell types in liver tumorigenesis. Our findings warrant the exploration of means to interfere with ST18-dependent epithelium-macrophage interactions in a therapeutic setting.

Introduction:

ST18 was originally identified as a candidate tumor suppressor in breast cancer, hence the name *"Suppression of Tumorigenicity 18"* (1). Successive studies revealed activation of the same gene in pediatric acute myeloid leukemia (2, 3) and hepatocellular carcinoma (HCC) (4), suggesting an oncogenic function of *ST18*. In particular, the mapping of integration sites of the endogenous retrotransposon L1 in hepatocellular carcinoma (HCC) led to the identification of 12 tumor-specific L1 insertions, one of which activated *ST18* (4).

ST18 (also called NZF-3 or MYT3) is a member of the *NZF/MyT1* family of transcription factors, a non-classical zinc finger family that includes two other members, neural zinc finger

factor-1 (NZF-1) and myelin transcription factor-1 (Myt1), with six C_2HC-type fingers arranged in two main clusters, each of which might in principle bind DNA (1, 5, 6). The three genes are expressed in neural tissue and, based on expression patterns and over-expression experiments, are involved in the induction of neuronal differentiation (7). *ST18* is expressed at low levels in a number of different rat tissues (including liver) and is required for fatty acid- and cytokine-induced apoptosis in pancreatic ß-cells (8). Finally, RNA interference and mRNA profiling studies in human fibroblasts indicated that ST18 regulates pro-apoptotic and pro-inflammatory genes in response to TNF-α (5), although the relevance of these regulatory events in cancer remained unclear.

Here, we unravel a critical role for *ST18* in a mouse model of HCC based on the adoptive transfer of transformed mouse embryonic hepatoblasts (9). *ST18* was undetectable in either cultured cells or normal livers, but was induced in subcutaneous tumors under the control of inflammatory cues, and in particular Tumor-associated macrophages (TAMs). Systemic depletion of macrophages in recipient animals prevented *ST18* expression in transformed hepatoblasts, and impaired both tumor development and maintenance. Reciprocally, *ST18* knockdown in hepatoblasts delayed tumor progression or, when induced in pre-formed tumors, led to rapid tumor involution, associated with loss of TAMs and down-regulation of an inflammatory gene expression signature. Hence ST18 expression in the epithelial compartment contributes to the tight connection between inflammation and tumorigenesis in the liver (10).

Materials and methods

Isolation, culture, retroviral infection and subcutaneous transplantation of liver progenitor cells.

We derived hepatoblasts from the two mouse strains C57/JHsd (Harlan laboratories) and TRP53/C57 (Jackson laboratories), according to a protocol published previously (9). Liver cell suspensions from fetal livers of E 14.5-18.5 mice were diced and treated with Dispase (Gibco, 1000U/ml) for one hour at 37C°. The livers were dispersed into single cells by pipetting and filtrated trough a nylon mesh filter (pore size 100μm). The cellular pellet was washed with hypotonic lysis buffer (150 mM NH_4Cl, 10 mM $KHCO_3$, 100 μM EDTA) for 3 min at 4°C, centrifuged and put in ice. Purification of E-cadherin positive hepatoblasts was performed using the MACS® magnetic cell sorting system (Miltenyi) through indirect labeling with the rat anti-

mouse E-cadherin (ECCD-1) antibody (Calbiochem) (11). Before loading onto MACS MS size columns, liver cell suspensions were incubated with the antibody complex for 45 minutes at 4C°. Antibody complexes were prepared by incubating 4μg of ECCD-1 antibody with 20μl of immunomagnetic beads at room temperature for one hour. Eluted cells were plated onto laminin-coated plates (Sigma) in DMEM (Lonza), supplemented with 10% FBS NA (HyClone), 1% glutamine (Euroclone), 1% penicillin/streptomycin (Life Technologies), HGF (40ng/ml, Peprotech), EGF (20 ng/ml, Peprotech) and Dexamethasone (10^{-6}M, Sigma). After 48h, cultured hepatoblasts were transduced with a combination of retrovirus encoding for c-*myc*, oncogenic RAS (H-Ras^{V12}) or shp53. Human hepatocellular liver carcinoma cell line HepG2 (DSMZ) were grown in RPMI (Lonza) supplemented with 10% FBS NA (HyClone), 1% glutamine (Euroclone) and 1% penicillin/streptomycin (Life Technologies) under 5%CO_2 at 37°C.

To generate shRNA hairpins targeting both human and mouse ST18, 97bp oligonucleotides were designed using an online tool (http://euphrates.mit.edu/cgi-bin/shRNA/index.pl) and used as templates for PCR with the following primers: XhoI_fw (5'-CAG AAG GCT CGA GAA GGT ATA TTG CTG TTG ACA GTG AGC G-3') and EcoRI_rv (5'- CTA AAG TAG CCC CTT GAA TTC CGA GGC AGT AGG CA-3'). Amplified PCR products were digested with XhoI/EcoRI and cloned in the mir-30 based retroviral vector TtRMPVIR (12). The target sequences used in this work are TTCATGCTTAAGTCCAATGtg (ST18_1), TTTAAAGACTGGATACTGCtg (ST18_6) and TTGATTCAGGAAATGGTGGtg (ST18_7). The efficacy of knock down was initially tested in 293T cells. Retroviruses were produced in Phoenix packaging cells and collected in DMEM (Lonza) supplemented with 10% tetracycline-free FBS NA (HyClone), 1% glutamine (Euroclone), 1% penicillin/streptomycin (Life Technologies). Supernatant was passed through a 0.45 μm filter and supplemented with polybrene (2μg/ml, Sigma). The infection procedure was repeated three times every 4 hours, before adding fresh medium supplemented with HGF (40ng/ml, Peprotech), EGF (20 ng/ml, Peprotech) and Dexamethasone (10^{-6}M, Sigma).

For *in vivo* tumor formation experiments, 3×10^5 genetically modified hepatoblasts were injected subcutaneously into CD1-nude mice (Charles River) in a volume of 0.3ml of PBS. Animals were monitored (2x per week) for signs of distress or disease and tumor size was measured using a caliper. *Ex vivo* imaging of Venus fluorescence in dissected tumors (Fig. 2B

and C) was performed on an IVIS Lumina III platform and analysed with the Living Image Software, version 4.2 (Caliper Life Sciences). Average radiant efficiency was calculated based on the epi-fluorescence signal, as indicated in the user manual.

Experiments involving animals were performed in accordance with the Italian laws (D.L.vo 116/92 and following additions), which enforces the EU 86/609 directive (Council Directive 86/609/EEC of 24 November 1986 on the approximation of laws, regulations and administrative provisions of the Member States regarding the protection of animals used for experimental and other scientific purposes).

Macrophage depletion *in vivo* and culture *in vitro*

To deplete macrophages *in vivo*, we used the anti-CSF-1R antibody (ASF98), a rat monoclonal anti-murine CD115 antibody (IgG2a) that inhibits CSF-1-dependent cell growth by blocking the binding of CSF-1 to its receptor (CSF-1R) and its selectivity has been previously characterized (13). As control we injected an isotype-matched anti Rat IgG (Sigma-Aldrich). Mice were injected i.p. at doses of 2 mg/mouse.

Clodronate, encapsulated in liposomes, was also used to deplete macrophages in $Mdr2^{-/-}$ and CD1-nude mice. Clodronate liposomes were prepared as described earlier (14). Control liposomes contained phosphate-buffered saline (PBS) only. Each animal received 0.01 mL/g (5 mg of clodronate per 1 mL of the total suspension volume) of clodronate liposomes or control liposomes via i.p. injection. The clodronate and control liposomes were obtained from the Foundation Clodronate Liposomes, Amsterdam, The Netherlands.

The murine macrophage cell line RAW264.7 (ECACC) were grown in DMEM (Lonza) supplemented with 10% FBS NA (HyClone), 1% glutamine (Euroclone) and 1% penicillin/streptomycin (Life Technologies) under 5%CO_2 at 37°C. Normal bone marrow macrophages were derived from of C57/BL6 mice (Harlan) (15).

Other methods

Other protocols and reagents are described online in Supporting Materials and Methods.

Results

We used a model based on the genetic manipulation of embryonic liver progenitors (hepatoblasts) *ex vivo* followed by their adoptive transfer into recipient mice (9). Hepatoblasts were isolated from fetal livers at embryonic days (E) 14.5-18.5 and transduced with different combinations of retroviruses expressing c-*myc*, oncogenic Ras (H-Ras^{V12}) or an shRNA targeting p53 (unless using p53-null cells). As expected (9), these cells became immortal in culture and acquired a transformed phenotype, as shown by their ability to generate liver-derived tumors with histological subtypes (16) and markers characteristic of human HCC when injected subcutaneously in immunocompromised CD-1 nude mice (Supporting Figs. S1A, B). RNA analysis and immunostaining revealed that *ST18* was expressed in tumors, but neither in normal liver (1, 8), nor in transformed hepatoblasts *in vitro* prior to injection into recipient mice (Fig. 1A), indicating that the gene was induced by tumor-associated micro-environmental signals.

ST18 is expressed in tumors arising in mice knockout for the *Abcb4* or *Mdr2* gene (henceforth *Mdr2$^{-/-}$* mice) (4), a model of inflammation-driven HCC (17). Pre-neoplastic livers in 4-10 months old *Mdr2$^{-/-}$* animals also became positive for ST18 (Fig. 1B), suggesting that expression was triggered by chronic inflammation even before the onset of tumorigenesis. *Mdr2$^{-/-}$* mice lack a P-glycoprotein of the bile canalicular membrane, causing defective secretion by hepatocytes of lipids required to neutralize bile salts (17). The ensuing high concentration of monomeric bile salts causes persistent damage of the hepatic epithelium forming the initial bile canaliculi, with the consequent inflammatory response preceding tumor development (18-20). These lesions are analogous to those observed in progressive familial intrahepatic cholestasis (PFIC), a recessive autosomal disorder involving a chronic hepatic inflammation that progresses to fatal liver failure during childhood. PFIC comes in three types, PFIC1, PFIC2 and PFIC3, with mutations in the hepatocyte membrane transporters ATP8B1, ABCB11 and ABCB4, respectively (21). The most severe form, PFIC2, may further progress to HCC or cholangiocarcinoma (22). Liver biopsies from PFIC1, PFIC2 and PFIC3 patients showed expression of ST18 in the three conditions, clearly above the levels detected in control tissue (Fig. 1C). Hence, membrane transporter deficiencies lead to analogous effects in mice and humans, with chronic inflammation and induction of ST18 expression.

p. 7

To further dissect the link between inflammation and ST18 expression, we induced an acute inflammatory response in wild-type C57BL/6 mice by intra-peritoneal injection of bacterial lipopolysaccharide (LPS) (23). ST18 was induced in the liver 24 hours after LPS injection, especially nearby blood vessels (Fig. 1D). Thus, either acute or chronic inflammatory conditions could trigger ST18 expression in liver cells, owing most likely to the exposure to pro-inflammatory cytokines or cellular contacts.

Based on above results, we hypothesized that expression of ST18 in hepatoblast-derived tumors (Fig. 1A) might be driven by the inflammatory microenvironment characteristic of many cancers (10, 24). Tumor-associated macrophages (TAMs) have been shown to play important cancer-promoting functions in a variety of models, including HCC (25, 26). Consistent with this notion, we observed significant infiltration of TAMs in mouse hepatoblast-derived tumors, as measured by IHC for the pan-macrophage marker Iba1 (27) (Supporting Fig. 1C). To mimic the interplay between macrophages and liver cancer cells *in vitro*, we co-cultured transformed hepatoblasts for 12 hours with either primary bone marrow-derived macrophages or the macrophage cell line RAW 264.7, and purified back liver cells before RNA isolation. Co-culture led to the acute induction of the *ST18* mRNA in hepatoblasts, which was further reinforced by pre-treatment of the macrophages with LPS for 1h (Supporting Fig. 1D). Milder activation of the gene was also observed upon treatment of hepatoblasts with RAW 264.7 culture supernatants (Supporting Fig. 1E). Thus, macrophages trigger ST18 induction in liver cells *in vitro*: this involves at least in part soluble cues, but remains most effective with cell-cell contacts.

To address the role of *ST18* in tumorigenesis, c-*myc*- and H-Ras^{V12}-transformed p53$^{-/-}$ hepatoblasts were transduced with an shRNA hairpin targeting *ST18* (expressed from the doxycycline-inducible vector TtRMPVIR) (12), sorted for expression of the associated Venus marker and injected subcutaneously into CD-1 nude mice. Induction of ST18 knockdown by exposure to doxycycline from the day of seeding (day 0) significantly suppressed tumor development relative to either untreated mice (shST18 off) or tumors infected with the control vector (shREN.713) (Supporting Fig. 2A, B). Thus, expression of ST18 is required for tumor development *in vivo*.

We then let tumors develop for two weeks before inducing the knockdown: four hours after activation, the *ST18* shRNA caused hemorrhages that progressively extended from the tumor site

to adjacent subcutaneous areas (Fig. 2A). Dissection and *ex vivo* imaging 24 hours after shRNA activation revealed hemorrhagic and friable tumor masses with loss of Venus fluorescence relative to untreated controls (Fig. 2B). RNA analysis and IHC staining confirmed a decrease in *ST18* abundance with residual expression confined to the progressively reduced non-necrotic areas (Fig. 2C, D). Similar effects were induced by two other *ST18* shRNAs, but not the shREN.713 control (Supporting Fig. 3A-D). Closer pathological analysis (Fig. 2E, insets) showed that in untreated mice, the subcutaneous tumor mass was consistent with a poorly differentiated tumor, composed of highly cohesive atypical cells. Doxycycline treated tumors showed severe intra-tumoral hemorrhages and necrotic areas that increased over time. Cells became multifocally less cohesive, arranged in bundles, and spindle-shaped. Staining with the vascular endothelial cell marker VE-cadherin (28) revealed a dilatation of intra-tumoral blood vessels (ectasia), coincident with a decrease in Ki67 and appearance of cleaved Caspase 3, none occurring with the control shRNA (Supporting Fig. 4A, B). Altogether, silencing of *ST18* led to proliferative arrest and induction of apoptosis, concomitant with vascular ectasia and hemorrhage: these combined effects are all likely to contribute to acute tumor regression.

Knockdown of ST18 in liver cancer cells also led to a rapid loss of TAMs in subcutaneous tumors, residual IBA1+ cells showing dramatic changes in morphology suggestive of impaired functionality (Supporting Fig. 4C, D). Importantly, TAMs themselves did not express ST18, and our experimental system ensures hepatocyte-specific knockdown. Thus, the maintenance of TAMs relied on sustained expression of ST18 in cancer cells.

To further investigate the interplay between ST18 expression in hepatoblasts, TAMs and tumor maintenance, we pre-depleted macrophages systemically in recipient animals by intra-peritoneal injection of a monoclonal antibody that blocks the murine CSF-1 receptor (or CD115) (13) or isotype-matched IgG as control. AntiCD-115 effectively caused selective depletion of circulating CD115$^+$ cells already 4 days after injection, with no effects on LY6G$^+$ neutrophils (Fig. 3A). At this stage (Day 0, Fig. 3B), transformed hepatoblasts were injected subcutaneously: examination of the animals over time showed continued depletion of circulating CD115$^+$ monocytes/macrophages (Fig. 3B), associated with a significant delay in tumor development (Fig. 3C). At day 15, CD115+ cell numbers were minimal and tumors virtually undetectable. At the last time-point (day 24) partial recovery of circulating CD115$^+$ cells (Fig. 3B) was accompanied by the growth of small tumor masses (Fig. 3C): relative to untreated controls,

however, these tumors still lacked macrophages (assessed by IBA1 staining), failed to induce ST18 and showed elevated apoptosis (Fig. 3D). Hence, macrophages are required for ST18 induction and tumor development.

We then addressed the effect of macrophage depletion in pre-formed tumors by injecting anti-CD115 or control IgG in tumor-bearing animals. Four hours after treatment, loss of IBA1$^+$ cells was accompanied by down-regulation of ST18, with intra-tumoral and subcutaneous hemorrhages (Fig. 3E, F). As an independent means to deplete macrophages, we injected liposome-encapsulated clodronate (14). Again, loss of IBA1$^+$ cells coincided with dramatic changes in tumor morphology, with necrosis, hemorrhage, loss of ST18 expression, and induction of apoptosis (Supporting Fig. 5A). Finally, we injected clodronate in pre-neoplastic and neoplastic $Mdr2^{-/-}$ animals, once again causing the parallel loss of IBA1 and ST18 staining (Supporting Fig. 5B, C). Altogether, we conclude that TAMs are required both for ST18 expression in cancer cells and tumor development/maintenance.

To complement our findings, we addressed the function of *ST18* in the human HCC cell line HepG2 since, unlike mouse hepatoblasts, these cells expressed *ST18* constitutively in the absence of inflammatory stimuli (4). *ST18* knockdown in cultured HepG2 cells induced cell death (Supporting Fig. 6A, B), indicating a cell-autonomous requirement for ST18. As with mouse hepatoblasts, induction of the shRNA in subcutaneous HepG2 tumors caused intra-tumoral hemorrhages and tumor regression (Supporting Fig. 6C-E).

We finally profiled ST18-dependent gene expression in our mouse model. RNA-seq analysis of control and ST18-depleted tumors (analyzed 4 hours following induction of shST18-6) allowed us to identify 677 and 467 up- and down-regulated genes, respectively (Tables S1, S2). The latter included known inflammation-related genes, such as members of the NF-kB family of transcription factors, as well as inflammatory cytokines and chemokines (most notably Ccl2) that are known to control the recruitment and activation of myeloid cells to the tumor sites (Fig. 4A) (29-33). Gene Set Enrichment Analysis (GSEA; Supporting Tables S3, S4) showed that ST18 knockdown led to the down-regulation of inflammation-associated genes, including in particular a set of genes up-regulated in hepatic stellar cells after stimulation with LPS (34) (Fig. 4B) as well as genes containing the binding motif for the inflammatory transcription factor NF-kB (Fig. 4C). Use of the Ingenuity pathway analyzer software further pointed to a role of the

transcription factor NF-kB in the regulation of ST18-dependent genes (Fig. 4C). Analysis of the NF-kB subunits P65 and P50 by immunostaining revealed rapid decreases in the levels of both proteins following ST18 knockdown (Fig. 4D, E) a result confirmed for p65 in macrophage-depleted tumors (Fig. 4E, Anti-CD115). While the mechanisms linking ST18 and NF-kB activities remain to be addressed, and indirect effects due to macrophage loss cannot be excluded at this stage, these data point to a role of ST18 upstream of NF-kB in controlling the transcriptional response of liver cells to inflammatory cues, thereby sustaining the mutual interaction between tumor cells and TAMs.

Discussion

Previous observations, including LINE-1 (L1) insertional mutagenesis in human Hepatocellular Carcinoma (HCC), as well as gene amplification and activation in inflammation-driven HCC nodules in *Mdr2-/-* mice, pointed to *ST18* as a candidate oncogene in hepatocellular carcinoma (4). However, direct evidence for a role of *ST18* in cancer was missing altogether. Using a mouse model of HCC based on *ex vivo* transformation and adoptive transfer of liver progenitor cells (hepatoblasts) (9), we demonstrate that ST18 is important for tumor development and maintenance. Detailed analysis revealed an unexpected mode of action for ST18, as a central component in a feed-forward loop between neoplastic epithelial cells and tumor-associated macrophages (TAMs).

The *ST18* mRNA and protein were undetectable in either normal liver (1, 8) or cultured hepatoblasts, but were expressed in subcutaneous tumors derived from the same cells. These results led us to hypothesize that *ST18* expression *in vivo* may require tumor-derived micro-environmental signals and in particular inflammatory infiltrates, a recurrent feature in solid tumors (10, 26). In line with this concept, hepatoblast-derived tumors contained infiltrating macrophages, ablation of which led to rapid down-regulation of ST18 in the tumor cells. Furthermore, *ST18* could be induced in liver cells, either *in vitro* by co-culture with macrophages, or *in vivo* by exposure to inflammatory conditions. Altogether, we conclude that *ST18* expression in tumors is triggered by inflammatory cues emanating from TAMs.

The role of *ST18* in tumor cells was addressed through inducible knockdown of the gene in the transduced hepatoblasts: this led to rapid tumor involution, associated with a series of catastrophic events (see below), among which a marked loss of TAM infiltrates. This mutual

dependency between expression of ST18 in hepatoblasts and maintenance of TAMs pointed to a regulatory loop between both cell types, with a central role in tumor maintenance. Indeed, the alternative modalities of intervention used in our experiments - ST18 knockdown in tumor cells vs. ablation of TAMs - had strikingly similar consequences. Both treatments suppressed tumor progression (compare Supporting Fig. 2 and Fig. 3C, D) or, if applied to pre-formed tumors, caused rapid tumor involution, associated with loss of TAMs (Supporting Fig. 4C, D and Fig. 3E), down-regulation of ST18 (Figs. 2D and 3E), proliferative arrest and apoptosis in the tumor cells (Supporting Fig. 4A and Fig. 3D), as well as pervasive hemorrhage, spreading from the tumor into the adjacent subcutaneous areas (Figs. 2A and 3F).

The precise origin of the TAMs infitrating subcutaneous tumor lesions remains to be determined. Like most tissues, both the liver and the skin are home to resident macrophage populations, which are intimately linked to tissue homeostasis and recruit blood monocytes when damage occurs (26, 35). At the steady state, most tissue-resident macrophage populations (with some notable exception such as the intestine and, to some extent, the liver) are originated during embryonic development by yolk-sac derived precursors, with minimal contribution from adult bone marrow hematopoiesis. The contribution of circulating monocytes to the resident macrophage pool is instead dominant in inflammatory contexts, such as infection and cancer (33, 35-38).

Notwithstanding the origin of TAMs, a large body of literature indicates that these cells - in particular in the M2 polarized state - tend to have strong pro-tumoral activities in most cancer types (26, 29). In HCC, in particular, TAM infiltration was shown to correlates with poor prognosis (39). Our macrophage-depletion experiments with anti-CD115 or Clodronate directly support this notion, and are consistent with previous observations in glioblastoma and breast cancer (29, 40, 41): it remains to be addressed whether TAMs may also elicit expression of ST18 in those tumors. Reciprocally, whether ST18 controls TAM function elsewhere than in the liver remains unclear. It is noteworthy here that TAMs can either promote or antagonize tumor growth (29), which may conceivably also explain the contrasting roles attributed to *ST18* in cancer (1-4).

The signaling pathways through which TAMs elicit ST18 expression in tumor cells, and ST18 in turn feeds back to TAMs, also remain to be unraveled. Our RNA-seq analysis indicated that ST18 might regulate part of the transcriptional response to inflammatory signals in

hepatoblasts, in particular through its requirement for NF-kB activation. Indeed, among the genes showing ST18-dependent expression in our tumor model, we find a number of known NF-kB regulated genes that may have a direct role in TAM homeostasis. CCL2 and Cxcl2, for example, are both involved in the recruitment of inflammatory monocytes (and myeloid cells) to tumors (32, 33, 42). Other pro-inflammatory cytokines such as IL-1b, IL-6 and CSF3, have been shown to control the phenotype of tumor-elicited myeloid cells (43, 44). Although not investigated experimentally in this study, the reduced expression levels of these cytokines in ST18-depleted tumors supports a model whereby (*i.*) TAMs derive from circulating monocytes in our tumor model and (*ii.*) ST18 controls the expression of critical environmental factors that control the recruitment/activation of TAM

An essential question brought up by our work regards the primary outputs of the aforementioned regulatory loop in tumor maintenance, with two extreme - albeit not exclusive - possibilities. First, ST18 may have an intrinsic (cell-autonomous) role in proliferation and survival of tumor cells, as suggested by our *in vitro* data on the HepG2 cell line. In this setting the tumorigenic properties of TAMs in the liver would rely - at least in part - on their ability to elicit ST18 expression in tumor cells. Second, ST18 may act mainly in a non-autonomous manner, allowing the maintenance of TAMs, which in turn signal tumor cell proliferation/survival. This cell-extrinsic effect of ST18 on TAMs may thus be an important, if not the principal determinant of its tumor-promoting activity in the liver (4).

In either of the above scenarios, our findings lend further support to the concept that macrophage targeting may be an effective therapeutic strategy in liver cancer (26). Among others, macrophage depletion enhanced the anti-tumoral effects of the kinase inhibitor sorafenib (45) and the chemotherapeutic agent Trabectedin acted in part though its toxic effect of TAMs (46). Hence, elucidation of the molecular mechanisms through which ST18 mediates epithelium-macrophage interactions, bears significant potential for future therapeutic development.

Finally, the mutual relationship between macrophages and epithelial cells in liver tumorigenesis, as well as the involvement of ST18 - and possibly NF-kB - in this process, may have important counterparts in tissue homeostasis. Indeed, Clodronate-mediated depletion of Kuppfer cells impaired liver regeneration upon partial hepatectomy, due to loss of NF-kB activation (47). In the same conditions, direct inhibition of NF-kB in hepatocytes increased

apoptosis and decreased proliferation (48). It will thus be interesting to address whether, as shown here for TAMs, Kupffer cells mediate the activation of ST18 in the regenerating liver epithelium, and whether ST18 is required for activation of NF-kB following partial hepatectomy. It is tempting to speculate here that this role of ST18 may extend to other tissues, representing perhaps a conserved element of macrophage-epithelium interactions.

Figure Legends

Fig. 1. ST18 is induced by inflammatory cues in hepatoblasts. A, Left: quantitative RT-PCR analysis of *ST18* mRNA levels in adult liver, in cell lines derived from mouse liver progenitors (including E14.5 shp53-Myc, E14.5 shp53-Ras^{V12}, E14.5 Myc-Ras^{V12}, E18.5 shp53-Myc-Ras^{V12}, and E18.5 shp53-Ras^{V12}) and in subcutaneous tumors derived from the same cells. * p = 0.002; ** p = 0.0462. Right: ST18 is expressed in subcutaneous hepatoblast-derived tumors, but not normal liver. **B,** H&E: Hematoxylin and eosin staining shows portal inflammatory infiltrates in pre-neoplastic Mdr2$^{-/-}$ livers at the indicated ages. ST18: staining of IHC sections with ST18 antibodies shows positivity in Mdr2$^{-/-}$ but not WT livers. **C,** Hepatic lesions and ST18 positivity in liver biopsies from PFIC1, PFIC 2 and PFIC3 patients. **D,** Mouse liver sections 24 hours after LPS treatment, showing irregular hepatocyte arrangement, inflammatory infiltrates and induction of ST18, stronger nearby blood vessels (arrow) in both periportal and centrilobular zones.

Fig. 2. Expression of ST18 is required for tumor maintenance. A, Hemorrhages initiating from the tumor and extending to the adjacent subcutaneous areas are noticeable already 4h after *ST18* silencing and increase progressively throughout the indicated time-course. All experiments shown in this figure were performed with by induction of the shST18-6 hairpin with administration of Doxycycline (at time 0) by oral gavage. **B,** Left: *ex-vivo* fluorescent imaging of tumors dissected from either untreated recipient mice, or 24h after Doxycycline administration. The fluorescent Venus marker is constitutively expressed from the same TtRMPVIR vector (12) expressing Doxycycline-inducible shST18: loss of fluorescence after *ST18* knockdown is thus due to loss of the targeted cells. Right: quantification of average radiant efficiency in the same tumors shown in b. (** p = 0.0013). **C,** Quantitative RT-PCR analysis of *ST18* mRNA levels in tumors confirms knockdown already 4h after shST18 induction. **D,** Induction of shST18 induces hemorrhages and necrosis concomitant with a progressive decrease of *ST18* expression. Insets denote that in untreated mice, the tumor is composed of highly cohesive atypical cells; in doxycycline treated tumors, instead cells are multifocally less cohesive, arranged in bundles and spindle-shaped. Scale bars: 100 μm.

Fig. 3. Depletion of macrophages *in vivo* prevents *ST18* expression in hepatoblasts, and affects both tumor development and maintenance. A, FACS analysis of macrophages (CD115$^+$) and neutrophils (LY6G$^+$) in peripheral blood 4 days after injection of mice with Anti-

p. 15

CD115 (+), compared with injection of control IgG (-). The data represent the average and s.d. from 3 independent mice. *p = 0.01. Cell numbers are expressed relative to total white blood cells. **B,** Analysis of CD115^{+} cell numbers over time in one of the above animals (note that day 0 here is the 4th day after anti-CD115 treatment, i.e. the same time-point analysed in panel A). **C,** Left: tumor volumes in mice pre-treated mice with either control IgG (-) or anti-CD115 (+) at Days 15 and 24 after tumor seeding. Right: photographs of tumors dissected (at day 24) from carriers pre-treated with IgG (control) or anti- CD115^{+}, as indicated. **D,** H&E and IHC staining for the indicated proteins (IBA1, ST18, cleaved caspase 3) reveal hemorrhage, macrophage depletion, lack of ST18 expression and increased apoptosis in tumors arising in anti-CD115-treated, relative to IgG-treated mice. **E,** H&E and IHC staining 8h after anti-CD115 or control IgG injection in established tumors, revealing effects analogous to the above, including intra-tumoral hemorrhage and necrosis (H&E), decreased ST18 expression and - as expected - loss of IBA1^{+} macrophages. Mean numbers of IBA1^{+} cells in four different microscopic fields in anti-CD115 and IgG-injected tumors. ** p < 0.0001. Scale bars: 100 μm. **F,** Subcutaneous hemorrhages are noticeable as early as 4h after anti-CD115 injection in established tumors and become more severe over time.

Fig. 4. ST18 knockdown in hepatoblast-derived tumors affects inflammation- and NF-kB-associated genes. RNA-seq was used to identify genes whose expression was affected 4h after induction of ST18 knockdown with the shST18-6 hairpin in subcutaneous tumors, with three mice per condition. **A,** Genes involved in NF-kB signaling and/or positive regulation of myeloid cell activity that showed ST18-dependent expression. **B,** Gene Set Enrichment Analysis (GSEA) showing that genes induced by LPS in hepatic stellar cells (gene set SEKI_INFLAMMATORY_RESPONSE_LPS_UP) (34) were down regulated after *ST18* knockdown. The heatmap shows the relative expression of the mRNAs included in this gene set in hepatoblast-derived tumors, without (untreated) or with ST18 knockdown (4h Doxy) (three independent samples for each condition). **C,** GSEA revealing that genes containing the NF-kB binding motif (V$NFKAPPAB_01) were down-regulated after *ST18* knockdown. **D,** IPA (Ingenuity pathway analyzer) software pointed to a central role of NF-kB in the regulation of ST18-dependent genes. **E,** IHC staining of the NF-kB subunits P65 and P50 revealed rapid decreases in the levels of both proteins following ST18 knockdown. **F**, Immunofluorescent

detection of the NF-kB subunit P65 revealed its rapid decrease in hepatoblast-derived tumors following ST18 knockdown and macrophage depletion.

Disclosure of potential conflicts of interest

The authors do not declare potential conflicts of interest.

References:

1.   Jandrig B, Seitz S, Hinzmann B, Arnold W, Micheel B, Koelble K, Siebert R, et al. ST18 is a breast cancer tumor suppressor gene at human chromosome 8q11.2. Oncogene 2004;23:9295-9302.
2.   Steinbach D, Schramm A, Eggert A, Onda M, Dawczynski K, Rump A, Pastan I, et al. Identification of a set of seven genes for the monitoring of minimal residual disease in pediatric acute myeloid leukemia. Clin Cancer Res 2006;12:2434-2441.
3.   Steinbach D, Bader P, Willasch A, Bartholomae S, Debatin KM, Zimmermann M, Creutzig U, et al. Prospective validation of a new method of monitoring minimal residual disease in childhood acute myelogenous leukemia. Clin Cancer Res 2015;21:1353-1359.
4.   Shukla R, Upton KR, Munoz-Lopez M, Gerhardt DJ, Fisher ME, Nguyen T, Brennan PM, et al. Endogenous retrotransposition activates oncogenic pathways in hepatocellular carcinoma. Cell 2013;153:101-111.
5.   Yang J, Siqueira MF, Behl Y, Alikhani M, Graves DT. The transcription factor ST18 regulates proapoptotic and proinflammatory gene expression in fibroblasts. FASEB J 2008;22:3956-3967.
6.   Yee KS, Yu VC. Isolation and characterization of a novel member of the neural zinc finger factor/myelin transcription factor family with transcriptional repression activity. J Biol Chem 1998;273:5366-5374.
7.   Kameyama T, Matsushita F, Kadokawa Y, Marunouchi T. Myt/NZF family transcription factors regulate neuronal differentiation of P19 cells. Neurosci Lett 2011;497:74-79.
8.   Henry C, Close AF, Buteau J. A critical role for the neural zinc factor ST18 in pancreatic beta-cell apoptosis. J Biol Chem 2014;289:8413-8419.
9.   Zender L, Xue W, Cordon-Cardo C, Hannon GJ, Lucito R, Powers S, Flemming P, et al. Generation and analysis of genetically defined liver carcinomas derived from bipotential liver progenitors. Cold Spring Harb Symp Quant Biol 2005;70:251-261.
10.   Mantovani A, Allavena P, Sica A, Balkwill F. Cancer-related inflammation. Nature 2008;454:436-444.
11.   Nitou M, Sugiyama Y, Ishikawa K, Shiojiri N. Purification of fetal mouse hepatoblasts by magnetic beads coated with monoclonal anti-e-cadherin antibodies and their in vitro culture. Exp Cell Res 2002;279:330-343.
12.   Zuber J, McJunkin K, Fellmann C, Dow LE, Taylor MJ, Hannon GJ, Lowe SW. Toolkit for evaluating genes required for proliferation and survival using tetracycline-regulated RNAi. Nat Biotechnol 2011;29:79-83.
13.   Sudo T, Nishikawa S, Ogawa M, Kataoka H, Ohno N, Izawa A, Hayashi S, et al. Functional hierarchy of c-kit and c-fms in intramarrow production of CFU-M. Oncogene 1995;11:2469-2476.

14. van Rooijen N, Sanders A, van den Berg TK. Apoptosis of macrophages induced by liposome-mediated intracellular delivery of clodronate and propamidine. J Immunol Methods 1996;193:93-99.

15. Austenaa LM, Barozzi I, Simonatto M, Masella S, Della Chiara G, Ghisletti S, Curina A, et al. Transcription of Mammalian cis-Regulatory Elements Is Restrained by Actively Enforced Early Termination. Mol Cell 2015;60:460-474.

16. Thoolen B, Maronpot RR, Harada T, Nyska A, Rousseaux C, Nolte T, Malarkey DE, et al. Proliferative and nonproliferative lesions of the rat and mouse hepatobiliary system. Toxicol Pathol 2010;38:5S-81S.

17. Smit JJ, Schinkel AH, Oude Elferink RP, Groen AK, Wagenaar E, van Deemter L, Mol CA, et al. Homozygous disruption of the murine mdr2 P-glycoprotein gene leads to a complete absence of phospholipid from bile and to liver disease. Cell 1993;75:451-462.

18. Fickert P, Fuchsbichler A, Wagner M, Zollner G, Kaser A, Tilg H, Krause R, et al. Regurgitation of bile acids from leaky bile ducts causes sclerosing cholangitis in Mdr2 (Abcb4) knockout mice. Gastroenterology 2004;127:261-274.

19. Mauad TH, van Nieuwkerk CM, Dingemans KP, Smit JJ, Schinkel AH, Notenboom RG, van den Bergh Weerman MA, et al. Mice with homozygous disruption of the mdr2 P-glycoprotein gene. A novel animal model for studies of nonsuppurative inflammatory cholangitis and hepatocarcinogenesis. Am J Pathol 1994;145:1237-1245.

20. Katzenellenbogen M, Mizrahi L, Pappo O, Klopstock N, Olam D, Jacob-Hirsch J, Amariglio N, et al. Molecular mechanisms of liver carcinogenesis in the mdr2-knockout mice. Mol Cancer Res 2007;5:1159-1170.

21. Jacquemin E. Progressive familial intrahepatic cholestasis. Clin Res Hepatol Gastroenterol 2012;36 Suppl 1:S26-35.

22. Knisely AS, Strautnieks SS, Meier Y, Stieger B, Byrne JA, Portmann BC, Bull LN, et al. Hepatocellular carcinoma in ten children under five years of age with bile salt export pump deficiency. Hepatology 2006;44:478-486.

23. Zhong J, Deaciuc IV, Burikhanov R, de Villiers WJ. Lipopolysaccharide-induced liver apoptosis is increased in interleukin-10 knockout mice. Biochim Biophys Acta 2006;1762:468-477.

24. McAllister SS, Weinberg RA. The tumour-induced systemic environment as a critical regulator of cancer progression and metastasis. Nat Cell Biol 2014;16:717-727.

25. Grivennikov SI, Greten FR, Karin M. Immunity, inflammation, and cancer. Cell 2010;140:883-899.

26. Sica A, Invernizzi P, Mantovani A. Macrophage plasticity and polarization in liver homeostasis and pathology. Hepatology 2014;59:2034-2042.

27. Rehg JE, Bush D, Ward JM. The utility of immunohistochemistry for the identification of hematopoietic and lymphoid cells in normal tissues and interpretation of proliferative and inflammatory lesions of mice and rats. Toxicol Pathol 2012;40:345-374.

28. Dejana E. Endothelial adherens junctions: implications in the control of vascular permeability and angiogenesis. J Clin Invest 1996;98:1949-1953.

29. Ostuni R, Kratochvill F, Murray PJ, Natoli G. Macrophages and cancer: from mechanisms to therapeutic implications. Trends Immunol 2015;36:229-239.

30. De Filippo K, Dudeck A, Hasenberg M, Nye E, van Rooijen N, Hartmann K, Gunzer M, et al. Mast cell and macrophage chemokines CXCL1/CXCL2 control the early stage of neutrophil recruitment during tissue inflammation. Blood 2013;121:4930-4937.

31. Hamilton JA. Colony-stimulating factors in inflammation and autoimmunity. Nat Rev Immunol 2008;8:533-544.

32. Qian BZ, Li J, Zhang H, Kitamura T, Zhang J, Campion LR, Kaiser EA, et al. CCL2 recruits inflammatory monocytes to facilitate breast-tumour metastasis. Nature 2011;475:222-225.

33. Bonapace L, Coissieux MM, Wyckoff J, Mertz KD, Varga Z, Junt T, Bentires-Alj M. Cessation of CCL2 inhibition accelerates breast cancer metastasis by promoting angiogenesis. Nature 2014;515:130-133.

34. Seki E, De Minicis S, Osterreicher CH, Kluwe J, Osawa Y, Brenner DA, Schwabe RF. TLR4 enhances TGF-beta signaling and hepatic fibrosis. Nat Med 2007;13:1324-1332.

35. Ginhoux F, Jung S. Monocytes and macrophages: developmental pathways and tissue homeostasis. Nat Rev Immunol 2014;14:392-404.

36. Bain CC, Bravo-Blas A, Scott CL, Gomez Perdiguero E, Geissmann F, Henri S, Malissen B, et al. Constant replenishment from circulating monocytes maintains the macrophage pool in the intestine of adult mice. Nat Immunol 2014;15:929-937.

37. Gomez Perdiguero E, Klapproth K, Schulz C, Busch K, Azzoni E, Crozet L, Garner H, et al. Tissue-resident macrophages originate from yolk-sac-derived erythro-myeloid progenitors. Nature 2015;518:547-551.

38.   Hoeffel G, Chen J, Lavin Y, Low D, Almeida FF, See P, Beaudin AE, et al. C-Myb(+) erythro-myeloid progenitor-derived fetal monocytes give rise to adult tissue-resident macrophages. Immunity 2015;42:665-678.

39.   Zhu XD, Zhang JB, Zhuang PY, Zhu HG, Zhang W, Xiong YQ, Wu WZ, et al. High expression of macrophage colony-stimulating factor in peritumoral liver tissue is associated with poor survival after curative resection of hepatocellular carcinoma. J Clin Oncol 2008;26:2707-2716.

40.   Pyonteck SM, Akkari L, Schuhmacher AJ, Bowman RL, Sevenich L, Quail DF, Olson OC, et al. CSF-1R inhibition alters macrophage polarization and blocks glioma progression. Nat Med 2013;19:1264-1272.

41.   Fend L, Accart N, Kintz J, Cochin S, Reymann C, Le Pogam F, Marchand JB, et al. Therapeutic effects of anti-CD115 monoclonal antibody in mouse cancer models through dual inhibition of tumor-associated macrophages and osteoclasts. PLoS One 2013;8:e73310.

42.   Steele CW, Karim SA, Leach JD, Bailey P, Upstill-Goddard R, Rishi L, Foth M, et al. CXCR2 Inhibition Profoundly Suppresses Metastases and Augments Immunotherapy in Pancreatic Ductal Adenocarcinoma. Cancer Cell 2016;29:832-845.

43.   Marigo I, Bosio E, Solito S, Mesa C, Fernandez A, Dolcetti L, Ugel S, et al. Tumor-induced tolerance and immune suppression depend on the C/EBPbeta transcription factor. Immunity 2010;32:790-802.

44.   Chittezhath M, Dhillon MK, Lim JY, Laoui D, Shalova IN, Teo YL, Chen J, et al. Molecular profiling reveals a tumor-promoting phenotype of monocytes and macrophages in human cancer progression. Immunity 2014;41:815-829.

45.   Zhang W, Zhu XD, Sun HC, Xiong YQ, Zhuang PY, Xu HX, Kong LQ, et al. Depletion of tumor-associated macrophages enhances the effect of sorafenib in metastatic liver cancer models by antimetastatic and antiangiogenic effects. Clin Cancer Res 2010;16:3420-3430.

46.   Germano G, Frapolli R, Belgiovine C, Anselmo A, Pesce S, Liguori M, Erba E, et al. Role of macrophage targeting in the antitumor activity of trabectedin. Cancer Cell 2013;23:249-262.

47.   Abshagen K, Eipel C, Kalff JC, Menger MD, Vollmar B. Loss of NF-kappaB activation in Kupffer cell-depleted mice impairs liver regeneration after partial hepatectomy. Am J Physiol Gastrointest Liver Physiol 2007;292:G1570-1577.

48.   Iimuro Y, Nishiura T, Hellerbrand C, Behrns KE, Schoonhoven R, Grisham JW, Brenner DA. NFkappaB prevents apoptosis and liver dysfunction during liver regeneration. J Clin Invest 1998;101:802-811.

162x101mm (300 x 300 DPI)

A Untreated | 4h Doxy | 12h Doxy | 24h Doxy (shST18-6)

B Untreated / 24h Doxy — Epi-fluorescence

Radiant efficiency / Doxy − + / shST18-6

C *ST18* in tumors — mRNA levels relative to *RPLP0* / Doxy (h) 0 4 8 12 24

D Untreated | 4h Doxy | 8h Doxy | 12h Doxy | 24h Doxy (shST18-6, H&E, ST18)
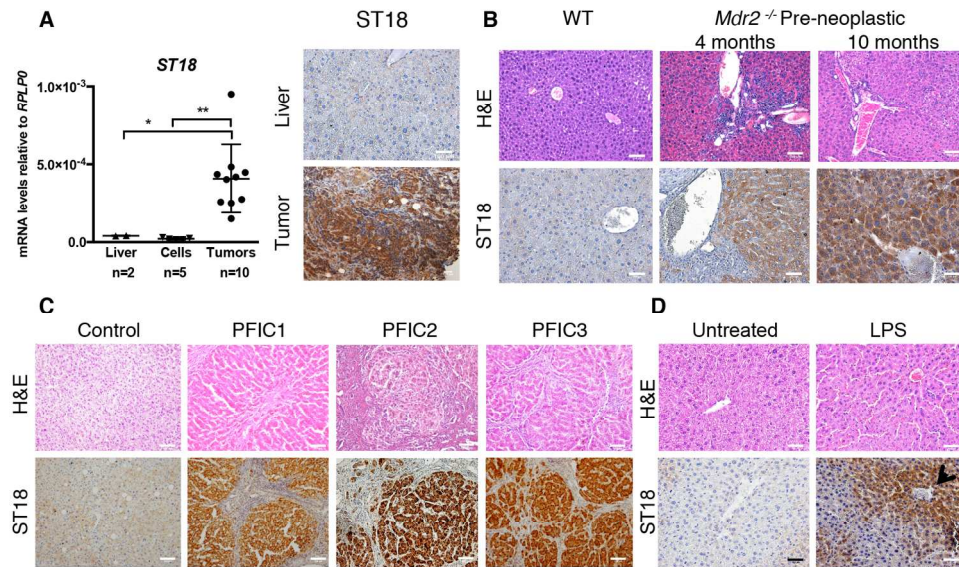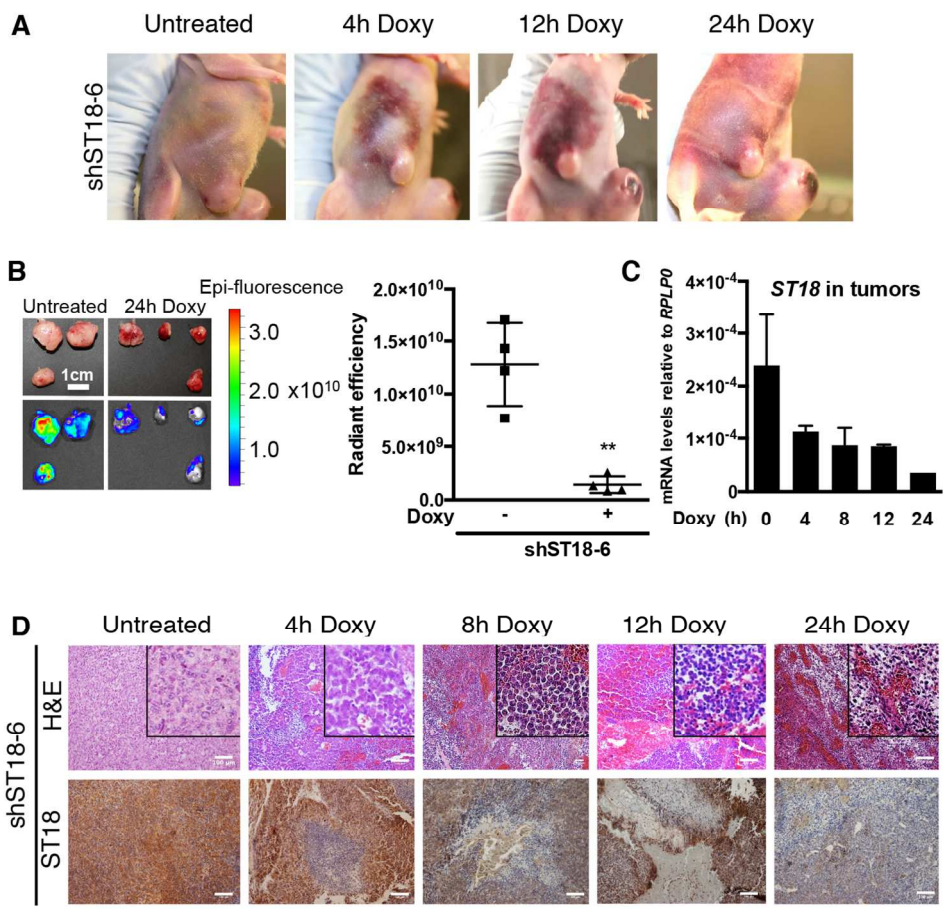
127x120mm (300 x 300 DPI)

113x203mm (300 x 300 DPI)

A

Gene name	Log2FC
Nfkb2	-0.64
Rela	-0.37
Relb	-0.79
Ccl2	-0.84
Ccl3	-1.24
Csf3	-1.06
Cxcl2	-0.96
Cxcl1	-1.15
Il1b	-0.68
Ccl20	-2.30
Il6	-0.51

B

C

Upstream Regulator	Predicted Activation State	Activation z-score	p-value of overlap
NFkB (complex)	Inhibited	-3.638	3.85E-08
RELA	Inhibited	-2.932	1.74E-05
NFKB1	Inhibited	-2.676	4.05E-03

D

E
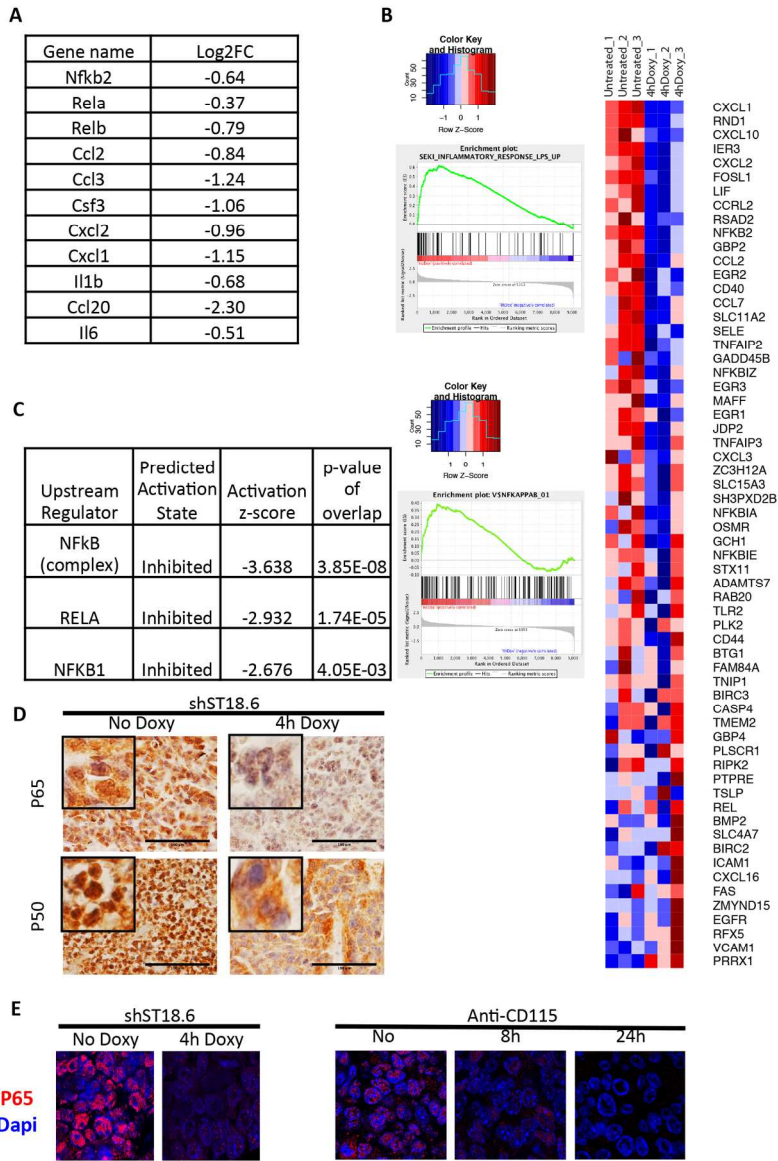
134x195mm (300 x 300 DPI)

Supplementa

Supplementa

Supplementa

Supplementa

ry Table 1: RNAseq analysis of control and ST18-depleted tumors identify 677 Differentially expressed ge

Column A: Annotated genes, indicated by their Gene Symbol

Columns B to D show differential expression as determined by RNA-seq. For each comparison, the log2Ratio and the q-value are provided. We identified 677 DEGs UP regulated genes in ST18 KD tumors as

ry Table 2: RNAseq analysis of control and ST18-depleted tumors identify 467 Differentially expressed ge

Column A: Annotated genes, indicated by their Gene Symbol

Columns B to D show differential expression as determined by RNA-seq. For each comparison, the log2Ratio and the q-value are provided. We identified 467 DEGs UP regulated genes in ST18 KD tumors as

ry Table 3: Gene Set Enrichment Analysis (GSEA) showed gene sets downregulated after ST18 Knockdow

Column A: Gene set name (GS)

Column B: Number of genes in the gene set (SIZE)

Column C: Enrichment score (ES)

Column D: Normalized Enrichment score (NES)

Column E: Nominal p value (NOM p-val)

Column F: False discovery rate (FDR q-val)

Column G: Familywise-error rate (FWER p-val)

Column H: Rank at Max. The position in the ranked list at which the maximum enrichment score occurred.

ry Table 4: Gene Set Enrichment Analysis (GSEA) showed gene sets upregulated after ST18 Knockdown.

Column A: Gene set name (GS)

Column B: Number of genes in the gene set (SIZE)

Column C: Enrichment score (ES)

Column D: Normalized Enrichment score (NES)

Column E: Nominal p value (NOM p-val)

Column F: False discovery rate (FDR q-val)

Column G: Familywise-error rate (FWER p-val)

Column H: Rank at Max. The position in the ranked list at which the maximum enrichment score occurred.

nes (DEGs) upregulated genes

• nes (DEGs) downregulated genes

n.

Mutual epithelium-macrophage dependency in liver carcinogenesis mediated by ST18

Ravà et al.

SUPPORTING INFORMATION

Supporting Materials and Methods

Doxycycline treatment

CD1-nude or Nod/Scid Hsd mice, injected with hepatoblasts (shp53, Myc, Ras^{V12}) containing the conditional shRNA vector (TtRMPVIR shST18) to silence ST18, were treated with Doxycycline to activate the knockdown of *ST18*. Mice were fed with 625mg/kg Doxycycline containing food (Mucedola). Additionally, we administrated the first dose of 200mg/ml Doxycycline (Sigma) in 300µl of water by oral gavage.

LPS treatment

C57/JHsd mice were injected intraperitoneally with 100 µg of lipopolysaccharide (LPS) and sacrificed 24h after treatment. Liver biopsies were dissected for pathological analysis.

Pathological and immunohistochemical analysis

Tumor or liver biopsies assigned to histological assessment were fixed in 4% formaldehyde overnight. The next day the samples were washed in 70% ethanol and subjected to paraffin embedding. 5 µm thick sections were stained with hematoxylin/eosin, and inspected by a mouse pathologist.

Human samples used in the study were obtained from formalin-fixed paraffin-embedded (FFPE) tissue from children diagnosed with PFIC1, PFIC2 or PFIC3. All specimens were obtained from native-liver hepatectomy performed during transplant surgery, carried out at the Hospital Papa Giovanni XXIII, Bergamo (Italy). Informed consent for the surgical procedure was obtained from the parents/carers. Formal approval for the use of the samples in the present work was provided by the local ethics committee (*Comitato Etico della Provincia di Bergamo*). All samples were kept strictly anonymous.

For Immunohistochemical analysis, 5 µm thick sections were de-waxed and re-hydrated through an ethanol scale, heated in EDTA (0.25mM, pH9, Dako #S2368) or citra solution

Ravà et al.   Supporting Information   p. 1

(BioGenex #HK086-9K) in a water bath at 99°C for 30 minutes for antigen unmasking, then left to cool down for 20 min, washed once in water and after 5 minutes, treated with 3% H_2O_2 for quenching of endogenous peroxidases. Slides were incubated with antibodies against Albumin (#106582, Abcam, 1:400), a-fetoprotein (#0008, Dako, 1:800), cytokeratin 19 (#901-242-012811, Biocare medical, 1:100), ST18 (#86563, Abcam, 1:200), Ki67 (#M7249, Dako, 1:500), Cleaved Caspase 3 (#9661, Cell Signaling, 1:200), Ve-Cadherin (#6458, Santa Cruz, 1:200), IBA1 (#019-19741, Wako, 1:1000), P65 (#86299, Abcam, 1:100) and P50 (#32360, Abcam, 1:200) in blocking solution (TBS containing 2% BSA, 2% goat serum, 0.02% Tween20) for 3h at RT. Slides were washed twice with TBS and incubated with the secondary antibody (DAKO Cytomation Envision System Labelled Polymer-HRP) for 45 minutes. After two additional washes in TBS, sections were developed with peroxidase substrate solution with DAB (DAKO) for 2-10 minutes. Slides were finally counterstained with hematoxylin, de-hydrated through alcoholic scale and mounted with Eukitt.

RNA extraction and analysis

Frozen tissue samples were homogenized with a dounce homogenizer or with the GentleMACS Dissociator (Miltenyi Biotec), depending on the tissue volume, prior to column extraction. RNA was extracted in Trizol (Invitrogen) using the RNeasy Mini Kit (Qiagen) according to the manufacturer's instructions. Quantification was performed on Nanodrop, and quality was assessed on Bioanalyzer (Agilent). 0.5 µg of total RNA was used for cDNA synthesis (using the ImProm-II Reverse Transcriptase, Promega), and 1 µl of the obtained cDNA was generally used as template for qPCR expression analyses. qRT-PCR (SYBR-green, Life Technologies) analysis was performed on an Applied Biosystems 7500 Real-time PCR system. Gene expression analyses by qRT-PCR were accomplished using the mouse/human *ST18* primers (F' GAAAACGGCACATTGGACTT; R' GGTGAGGAAGTTGGGGGTAT). Values were normalized to *RPLP0 (F'* TTCATTGTGGGAGCAGAC; R' CAGCAGTTTCTCCAGAGC). For RNA-seq, 5 µg of total RNA were depleted of ribosomal RNA with the Ribo-Zero™ rRNA Removal Kit from Epicentre®. Successful removal of ribosomal RNA was assessed using the BioAnalyser 2100. RNAseq libraries were prepared with the Illumina TruSeq RNA sample preparation kit v2 following the manufacturer's protocol. Briefly, RNA was fragmented and cDNA was synthesized, end-repaired and 3'-end-adenylated. Following adapter ligation, libraries were amplified by PCR for 15 cycles. Libraries with distinct TruSeq adapter indices were multiplexed (3 libraries per lane) on a HiSeq 2000 and sequenced for 50 bases in the paired-

Ravà et al.   Supporting Information   p. 2

end mode. Duplicated reads were eliminated using rmdup function from the suite samtools (http://samtools.sourceforge.net/). Differentially expressed genes were determined using the DESeq2 tool (15) available from Bioconductor with default parameters. Functional annotation was performed using the Gene Ontology categories of the bioinformatics tool Gene Set Enrichment Analysis (GSEA) based on Molecular Signatures Database (MSigDB). The dataset was deposited in the NIH GEO database under accession number GSE72403 (http://www.ncbi.nlm.nih.gov/geo/query/acc.cgi?token=kjgnciyupdkdbib&acc=GSE72403)

Flow cytometry and cell sorting

Primary hepatoblasts transduced with TtRMPVIR shRNA plasmids were monitored by flow cytometry for expression of the associated Venus marker without prior fixation, as single cell suspension in PBS. Cells were analyzed using a FACSCalibur (Becton-Dickinson; Mountain View, CA) flow cytometer. Macrophages were detected in peripheral blood with anti-mouse CD115 APC (#17-1152, eBioscience, 1:100). Neutrophils were detected with Anti-Mouse Ly-6G (#551459, BD Pharmingen 1:300). Liver progenitor cells, derived from E18.5 p53-null mice, transduced with retroviruses expressing c-*myc*, oncogenic Ras (H-Ras^{V12}) and shST18 (expressed from the vector TtRMPVIR) (12), were sorted for expression of the associated Venus marker using a Moflo Astrios (Beckman Coulter). All FACS data were analyzed using the FlowJo software (TreeStar).

Supporting Figure Legends

Supporting Fig. 1. Subcutaneous tumors derived from liver progenitor cells are of hepatic origin. **A,** Hematoxylin and eosin (H&E) stained sections show close resemblance of hepatoblast-derived subcutaneous tumors with different histological subtypes of human HCC (Solid, Pseudoglandular, Trabecular), as indicated above each panel. **B,** Tumor sections were stained for the liver progenitor markers albumin, α-fetoprotein, or cytokeratin 19. A representative subcutaneous tumor generated with shp53, Myc and Ras^{V12}-transduced E18.5 hepatoblasts is shown here as an example. All tumors examined in this study were positive for at least two of the three markers, confirming their liver origin. **C,** Staining for the pan-macrophage marker IBA1 (32) reveals abundant macrophage infiltration in subcutaneous tumors. All scale bars in A-D are 100 μm. **D.** *ST18* induction in hepatoblasts upon co-culture for 12h with normal bone marrow-derived macrophages (*p = 0.0020) or RAW 264.7 (**** p = 0.0008). Pre-treatment of the macrophages with LPS for 1h further augmented their *ST18*-inducing potential (**p = 0.0011 and ****p = 0.028 both relative to co-culture with untreated macrophages). Hepatoblasts were purified by sorting based on the Venus marker before RNA extraction and qRT-PCR. **E.** *ST18* induction in hepatoblasts by treatment with macrophage supernatant (1h). * p = 0.0367. Scale bars: 100 μm.

Supporting Fig. 2. ST18 expression is required for tumor development *in vivo*. A, Mice transplanted with c-*myc*- and H-Ras^{V12}-transformed p53$^{-/-}$ hepatoblasts expressing a doxycycline-inducible *ST18* shRNA hairpin (shST18-6) show reduced tumor development, compared with either non-induced shST18-6, or the control hairpin shREN.713. The photographs show three different mice per experimental condition, with Doxycycline used to induce either shST18-6 or shREN.713 from the day of seeding (day 0). **B,** Tumor volumes, measured at day 21, with (+) of without (-) induction of either shST18-6, or shREN.713 from day 0.

Supporting Fig. 3. ST18 depletion causes rapid hemorrhages *in vivo*. A, As Fig. 2A, and **B-D** as Fig. 2D, for two other ST18-specific shRNAs (shST18-1 and -7) and the shREN.713 control, as indicated. Scale bars: 100μm.

Supporting Fig. 4. Immunohistological analysis of subcutaneous tumors following *ST18* knockdown. **A,** Immunohistochemical staining reveals vascular ectasia (VE-cadherin), decrease in proliferation (Ki67) and apoptosis (cleaved Caspase 3) upon *ST18* silencing (with shST18-6 induced for 4h). **B,** None of the aforementioned changes occurred after induction

of the shREN.713 control. **C,** Staining for the macrophage marker IBA1 before (untreated) and after activation of shST18-6 or shREN.713, as indicated. *ST18* knockdown in the epithelial cells causes morphological changes in macrophages, in particular retraction of cytoplasmic processes and cellular rounding (insets). **D,** Reduction in macrophage numbers in shST18-6-expressing tumors after 4h (* $p = 0.0003$) and 8h (** $p = 0.0001$) of doxycycline treatment. Scale bars: 100μm.

Supporting Fig. 5. Clodronate-mediated depletion of macrophages *in vivo* confirms their crucial role for *ST18* expression. A, Tumor-bearing animals were treated with liposome-encapsulated clodronate. Three days after treatment loss of IBA1+ macrophages is accompanied by hemorrhage, loss of ST18 expression and induction of cleaved Caspase 3. **B, C,** Clodronate treatment in pre-neoplastic (**B,** 7 months) and neoplastic (**C,** 17 months) *Mdr2$^{-/-}$* mice causes reduced ST18 expression within 2 days. Scale bars: 100μm .

Supporting Fig. 6. *ST18* knockdown in HepG2 cells induces cell death *in vitro* and tumor regression *in vivo*. A, Quantitative RT-PCR analysis of mRNA levels in HepG2 cells shows expression of *ST18* at basal level and 24h after shST18 induction. Mouse hepatoblasts grown *in vitro* do not express ST18, and are shown for comparison. **B,** Activation of shST18 but not shREN.713 induces death of HepG2 cells, as measured by trypan blue staining. The shST18-6 hairpin, which targets both human and mouse *ST18*, was induced by Doxycyline treatment for the indicated periods of time. **C,** Hemorrhage and **D,** tumor regression following shST18 activation in subcutaneous HepG2 tumors. Following the seeding of 3×10^{5} HepG2 cells subcutaneously, tumors were left to develop in the recipient animals for 30 days, prior to doxycycline treatment (day 0). **E,** Tumors dissected following shST18 knockdown (shST18-6 ON, 24 hours after induction) show reduced sizes compared to either untreated mice (shST18 OFF) or to shREN.713 control tumors with or without doxycycline.
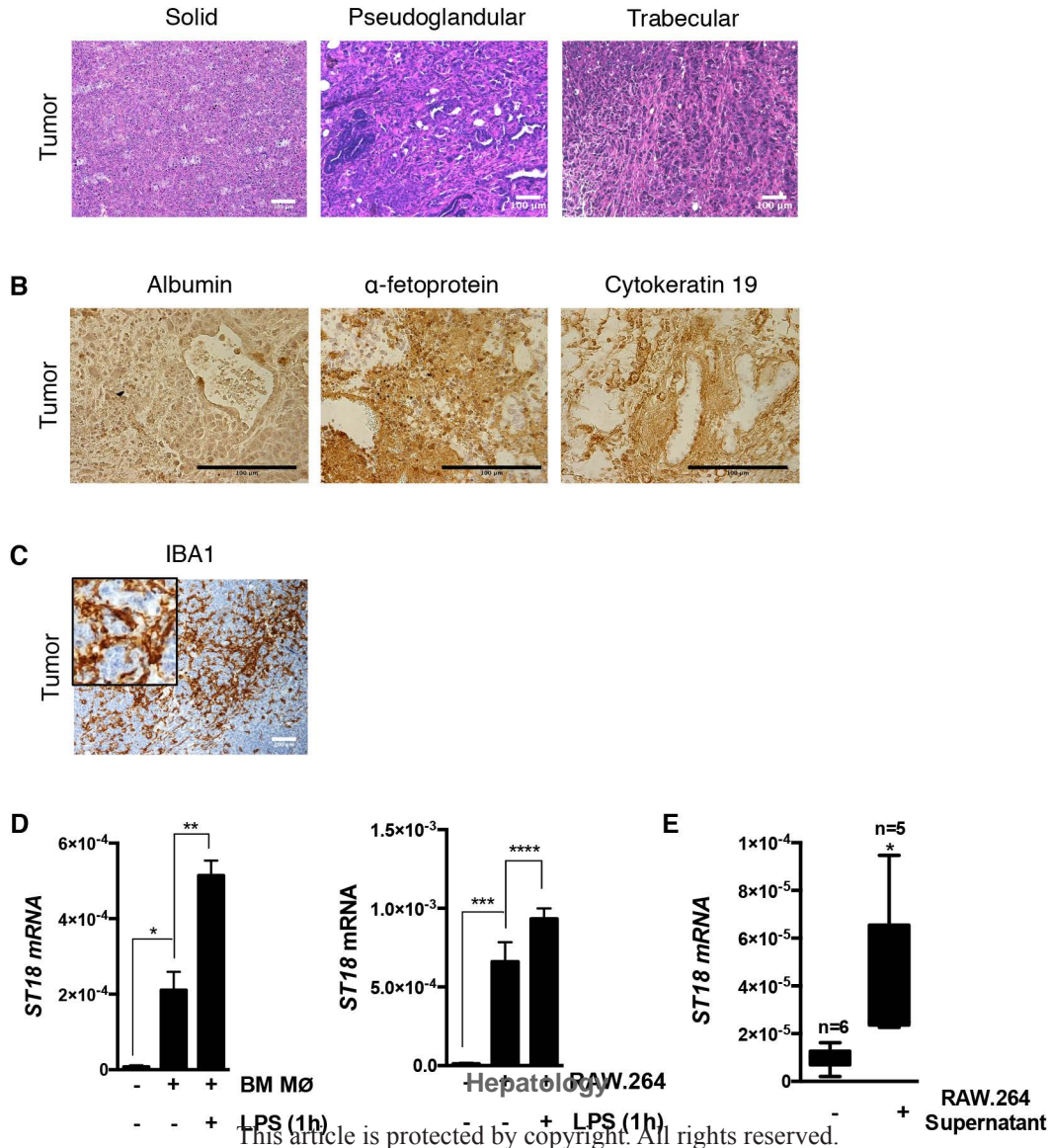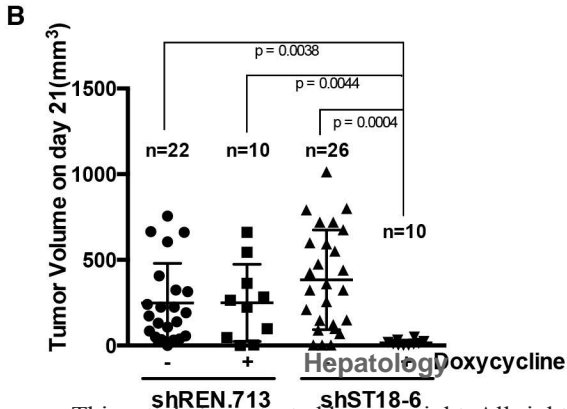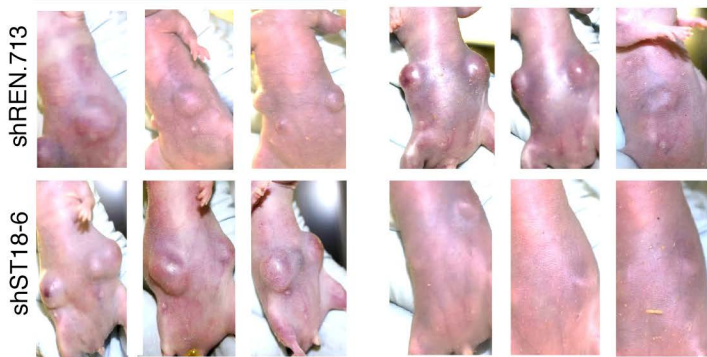
A

| Solid | Pseudoglandular | Trabecular |

B

| Albumin | α-fetoprotein | Cytokeratin 19 |

C

IBA1

D

E

Hepatology

A

| | H&E | IBA1 | ST18 | Cleaved Caspase 3 |

PBS
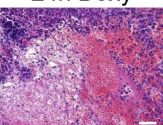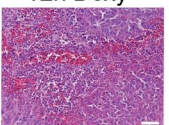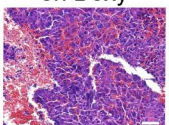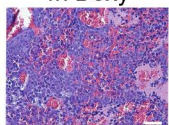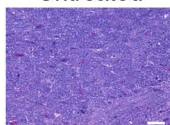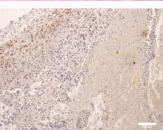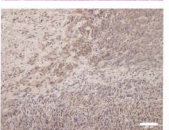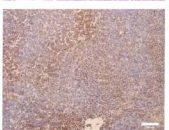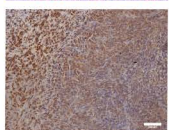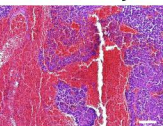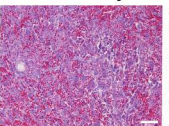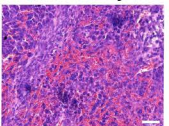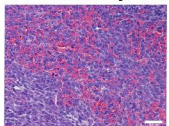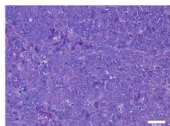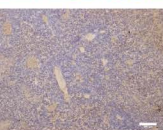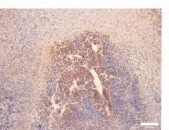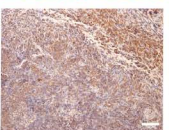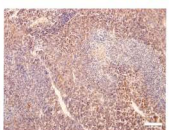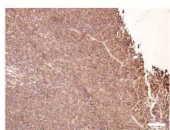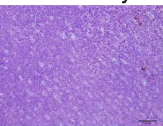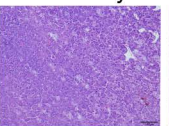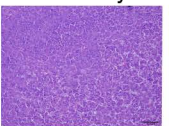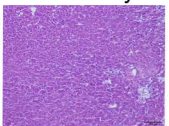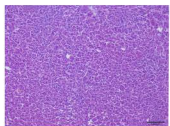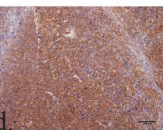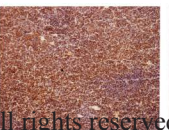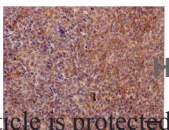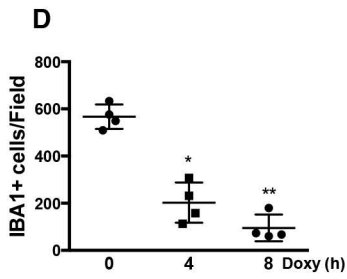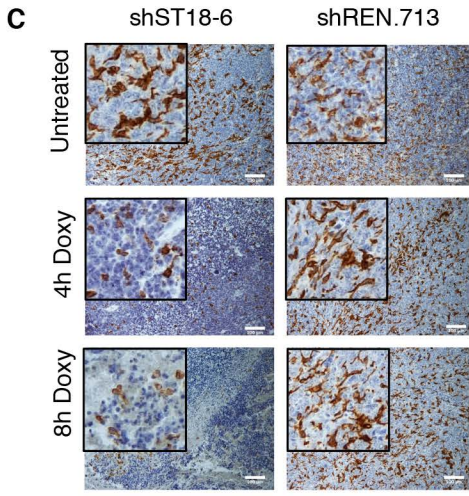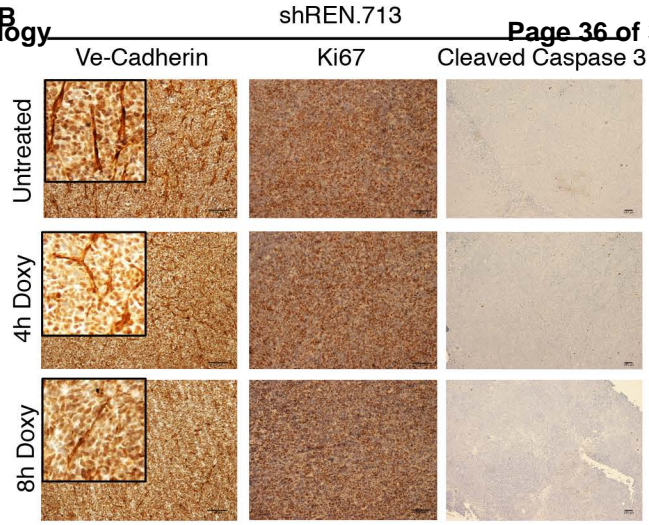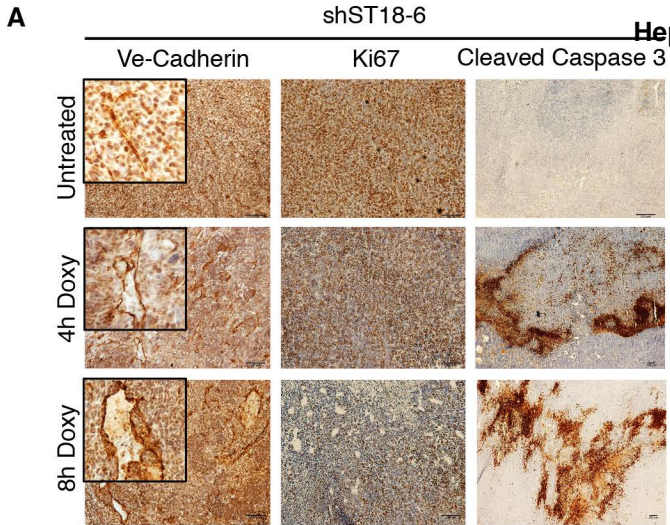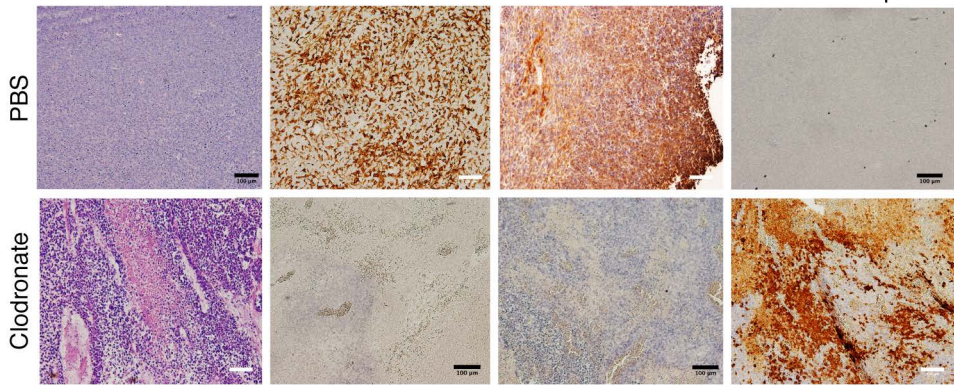
Clodronate
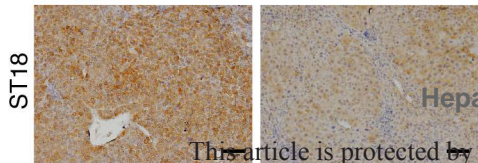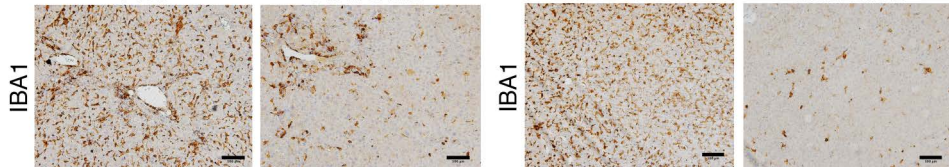
B Mdr2$^{-/-}$ Pre-neoplastic
PBS   Clodronate

C Mdr2$^{-/-}$ neoplastic
PBS   Clodronate

IBA1

ST18

A ST18

B Hepatology

C Untreated | Doxy 24h

D Tumor Volume (mm³) vs Days

shREN.713 on
shREN.713 off
shST18-6 on
shST18-6 off

E shST18-6 | shREN.713